ADVANCED MATERIALS
www.advmat.de

Investigation of Potassium Storage in Layered P3-Type $K_{0.5}MnO_2$ Cathode

*Haegyeom Kim, Dong-Hwa Seo, Jae Chul Kim, Shou-Hang Bo, Lei Liu, Tan Shi, and Gerbrand Ceder**

Novel and low-cost batteries are of considerable interest for application in large-scale energy storage systems, for which the cost per cycle becomes critical. Here, this study proposes $K_{0.5}MnO_2$ as a potential cathode material for K-ion batteries as an alternative to Li technology. $K_{0.5}MnO_2$ has a P3-type layered structure and delivers a reversible specific capacity of ≈100 mAh g^{-1} with good capacity retention. In situ X-ray diffraction analysis reveals that the material undergoes a reversible phase transition upon K extraction and insertion. In addition, first-principles calculations indicate that this phase transition is driven by the relative phase stability of different oxygen stackings with respect to the K content.

Rechargeable batteries have emerged as important devices for the storage of intermittent energy generated from renewable energy resources such as solar and wind. While Li-ion battery (LIB) technology has shown dominance in powering portable electronics and electric vehicles, it remains debatable whether the scarce resources for many of the metals in LIBs can satisfy the demands from large-scale application in grid-level storage.[1] This uncertainty has generated broad research interest into cost-effective alternatives. In this context, Na-ion batteries (NIBs) have been investigated as a promising option because of the abundance of Na and the similar chemistries of Na and Li systems.[1] However, there are two critical intrinsic problems associated with NIB technology: (i) the higher standard redox potential of Na/Na^+ usually translates into a lower working voltage than Li^+ and (ii) graphite, a conventional anode for LIBs, cannot reversibly intercalate Na ions, instead requiring the use of hard carbon anodes.[2] Thus, K-ion batteries (KIBs) with abundant K resources may be preferable as the standard redox potential of K/K^+ is lower than that of Na^+/Na, and graphite can store and release K ions.[3]

Reversible K-ion storage in various anode materials including carbonaceous materials (i.e., graphite, hard carbon, and graphene),[3,4] metals (i.e., antimony and tin),[5] metal oxides (i.e., $K_2Ti_8O_{17}$ and $K_2Ti_4O_9$),[6] and organic materials (i.e., potassium terephthalate and potassium 2,5-pyridinedicarboxylate) has been demonstrated.[7] However, only a limited number of cathode materials for KIBs have been reported to date,[8] making the development of appropriate cathode materials critical for practical application of KIBs. Layered transition metal oxides (TMOs) have been intensively studied for LIBs and NIBs because their close-packed structure leads to high volumetric energy density. In this respect, Vaalma et al. demonstrated the use of layered $K_{0.3}MnO_2$ as a positive electrode for K ions.[8b] Recently, Wang et al. also reported the use of $K_{0.7}Fe_{0.5}Mn_{0.5}O_2$ nanowires as a cathode for KIBs.[8c] These pioneering works demonstrate the potential of layered TMOs for KIBs and motivate the search for new layered TMO compounds.

In this study, we synthesized layered P3-type $K_{0.5}MnO_2$ and evaluated its electrochemical performance as a cathode for KIBs. Although the synthesis and structure of P3-type $K_{0.5}MnO_2$ have been previously reported,[9] its K-storage properties have not yet been investigated. We further investigate the structural changes of $K_{0.5}MnO_2$ upon K extraction and insertion using in situ X-ray diffraction (XRD) coupled with electrochemical titration and first-principles calculations. This work provides a better understanding of the underlying K-storage mechanism in layered P3-type $K_{0.5}MnO_2$ as well as insight for the design and development of novel cathode materials for KIBs.

Figure 1a presents an XRD pattern of the as-synthesized $K_{0.5}MnO_2$ and its refined profile assuming the presence of two phases with space groups of *R*3*m* and C*mcm*. The large background between 12° and 30° originates from the Kapton film used to seal the sample. The refined results indicate a P3-type layered structure (R3*m* space group) as major phase with a small amount of orthorhombic K_xMnO_2 impurity (≈6%) (C*mcm* space group). In the P3-type structure, oxygen ions form parallel layers stacked in ABBCCA sequence, with Mn ions occupying the octahedral sites, and K ions sitting in the prismatic sites

Dr. H. Kim, Dr. J. C. Kim, Dr. S.-H. Bo, Prof. G. Ceder
Materials Sciences Division
Lawrence Berkeley National Laboratory
Berkeley, CA 94720, USA
E-mail: gceder@berkeley.edu
Dr. D.-H. Seo, T. Shi, Prof. G. Ceder
Department of Materials Science and Engineering
University of California
Berkeley, CA 94720, USA
Dr. S.-H. Bo
University of Michigan–Shanghai Jiao Tong University Joint Institute
Shanghai Jiao Tong University
800 Dongchuan Road, Minhang District, Shanghai 200240, P. R. China
Dr. L. Liu
Department of Materials Science and Engineering
Massachusetts Institute of Technology
Cambridge, MA 02139, USA

DOI: 10.1002/adma.201702480

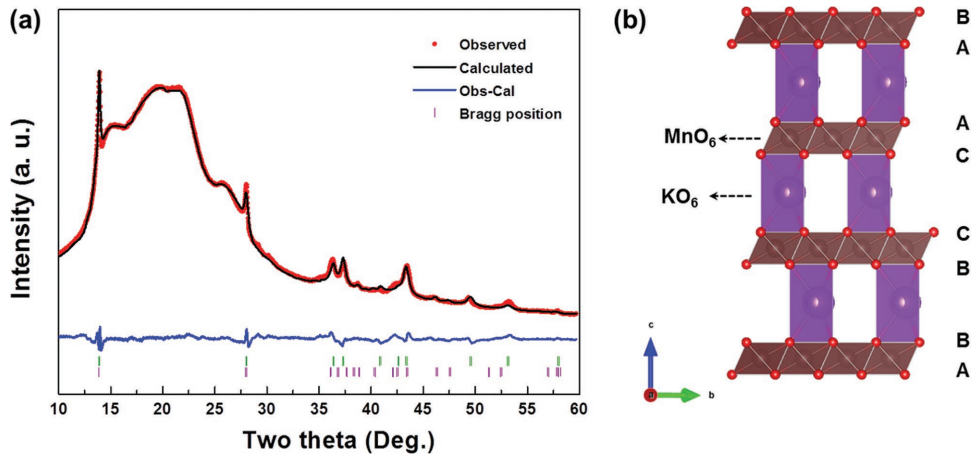

Figure 1. Structural characterization of P3-$K_{0.5}MnO_2$. a) Rietveld-refined XRD profile of as-prepared $K_{0.5}MnO_2$. The structure was refined assuming the coexistence of a majority R3*m* phase (green) and a minority C*mcm* phase (purple). $R_{wp} = 3.2$. b) Illustration of the P3-type $K_{0.5}MnO_2$ structure.

between the layers of MnO_6 octahedra, as shown in Figure 1b. The hexagonal lattice parameters of the major P3-$K_{0.5}MnO_2$ phase are refined to be $a = b = 2.875$ Å and $c = 19.085$ Å, which agree well with the values reported in the literature.[9] Using inductively coupled plasma-mass spectroscopy (ICP-MS) analysis, the K:Mn ratio in the sample was determined to be 0.48, close to the target composition of 0.5. The individual contributions of the target material and impurity phase to the K content in the sample cannot be distinguished using the ICP-MS technique. Therefore, we used density functional theory (DFT) calculations to determine the *c* lattice parameter of $K_{0.5}MnO_2$ as it is sensitive to the alkali ion concentration in layered TMOs.[10] The calculated *c* lattice parameter of 19.22 Å agrees well with the experimental result (within 1% error), which indicates that the K concentration (x) in the K_xMnO_2 sample is close to 0.5. Note that DFT calculations using the GGA+U approach slightly overestimate lattice parameters.[11] Examination of the powder with scanning electron microscopy (SEM) indicates that the average particle size of the as-prepared P3-$K_{0.5}MnO_2$ is 1–2 µm, as observed in Figure S1 in the Supporting Information.

The K-storage properties of P3-$K_{0.5}MnO_2$ were investigated using cyclic voltammetry and galvanostatic measurements, with the results presented in **Figure 2**. The open-circuit voltage (OCV) of the fresh P3-$K_{0.5}MnO_2$ cathode is ≈2.7 V (vs K/K^+). This OCV value is slightly lower than what is observed in $K_{0.3}MnO_2$ (OCV ≈ 3.1 V) reported by Vaalma et al.,[8b] likely due to the higher K content. When scanning between 1.5 and 4.2 V (vs K/K^+), two strong oxidation peaks are observed at ≈3.7 and 4.1 V (vs K/K^+), whereas the corresponding reduction peaks are less obvious (Figure 2a). In contrast, the oxidation and reduction peaks match well when scanning between 1.5 and 3.9 V, as observed in Figure 2b. These results imply that the K extraction and re-insertion processes may cause an irreversible structural change in the high-voltage region. Similar results are also obtained for galvanostatically cycling of the P3-$K_{0.5}MnO_2$ cathode. Figure 2c presents the voltage–capacity curves for the first four cycles at a current rate of 5 mA g^{-1} within the voltage range of 1.5–4.2 V (vs K/K^+). Two distinct plateau-like features are observed at ≈3.7 and ≈4.1 V (vs K/K^+) upon charging, whereas the voltage plateaus are less pronounced in the subsequent discharge cycles. The first charge and discharge capacities are 93 and 140 mAh g^{-1}, respectively, suggesting that although ≈0.39 K is removed, ≈0.57 K can be reinserted. Note that, higher specific capacity is achieved during discharge than during the first charge because the first charge process starts from the K-deficient phase ($K_{0.5}MnO_2$). When cycling between 1.5 and 3.9 V (Figure 2d), P3-$K_{0.5}MnO_2$ maintains a well-pronounced plateau at ≈3.6 V and delivers specific capacities of ≈53 and 106 mAh g^{-1} in the first charge and discharge, respectively. These results indicate that reversible K de/intercalation can be achieved by varying the K concentration (x) in K_xMnO_2 between ≈0.28 and ≈0.72. It should be noted that the voltage profile of P3-$K_{0.5}MnO_2$ shares features with that of $K_{0.3}MnO_2$,[8b] for which the structure is P2-type layered with an orthorhombic distortion. This implies that the potential is determined by the K content and distributions (such as K^+/vacancy ordering) in the K^+ layers, rather than by the polymorphism of MnO_2 stacking. In Figure 2e, we compare the capacity retention of P3-$K_{0.5}MnO_2$ cycled in the two voltage ranges. The high-voltage cycling (1.5–4.2 V) leads to substantial capacity fading; the capacity of P3-$K_{0.5}MnO_2$ at the 20th cycle is 47 mAh g^{-1}, which is ≈30% of its initial discharge capacity. To determine whether the poor cycling stability during the high-voltage cycling originates from a kinetic limitation or degradation of the material, we compared the cycling stability of P3-$K_{0.5}MnO_2$ at room temperature to that at 45 °C. As observed in Figure S2 in the Supporting Information, cycling at elevated temperature does not increase the achievable capacity but leads to severe capacity fade. This finding indicates that the capacity degradation during the high-voltage cycling is likely attributable to destabilization of the charged structure of P3-$K_{0.5}MnO_2$. The instability of P3-$K_{0.5}MnO_2$ upon high-voltage cycling at 1.5–4.2 V is further confirmed from our ex situ XRD analysis. Figure S3 in the Supporting Information shows the XRD pattern of P3-$K_{0.5}MnO_2$ after ten cycles. The typical set of diffraction peaks for the layered structure, usually observed between 15° and 30°, are missing indicating that a large portion of the phase becomes amorphized or at least loses any periodicity along the *c*-direction. In contrast, cycling between 1.5 and 3.9 V resulted in much better cycling performance for the P3-$K_{0.5}MnO_2$

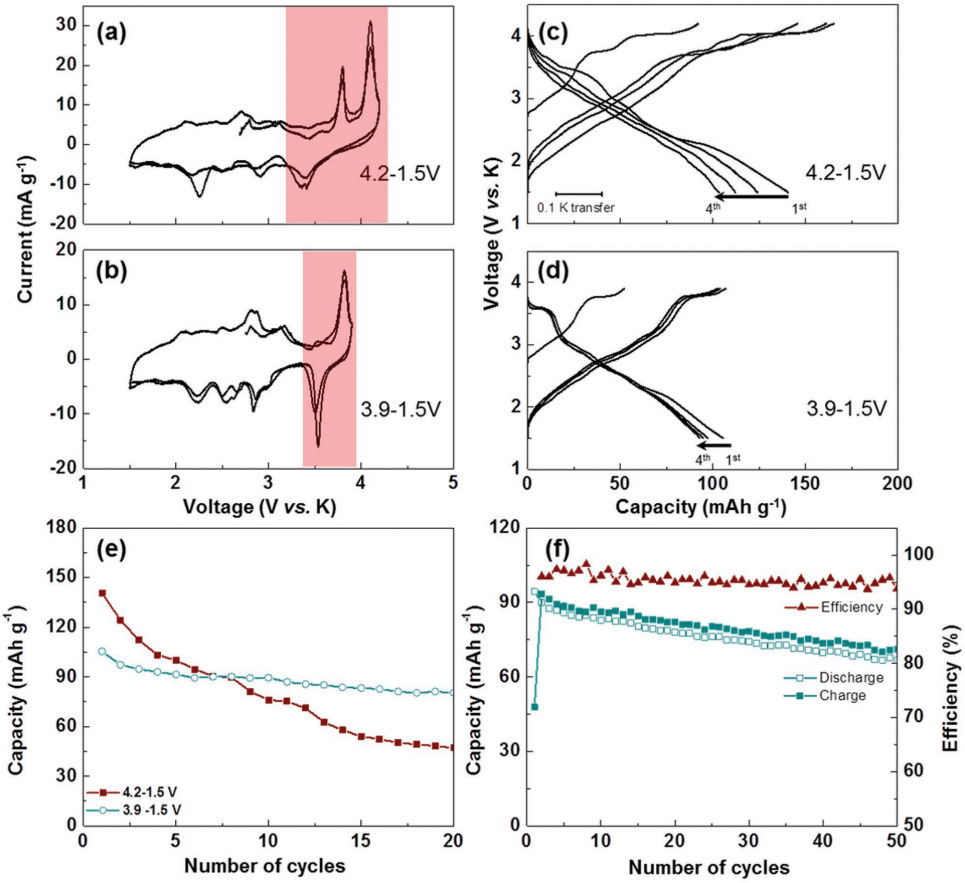

Figure 2. K-storage properties of P3-$K_{0.5}MnO_2$. a,b) Cyclic voltammograms at a scan rate of 0.03 mV s^{-1} and c,d) galvanostatic voltage–capacity profiles of P3-type $K_{0.5}MnO_2$ with two different voltage cutoffs. e) Discharge capacity of P3-type $K_{0.5}MnO_2$ over 20 cycles with the two different voltage cutoffs at a current rate of 5 mA g^{-1}. f) Cycle stability and coulombic efficiency (of the first discharge) of P3-type $K_{0.5}MnO_2$ at a current rate of 20 mA g^{-1} in the range of 3.9–1.5 V (vs K/K^+).

cathode; a discharge capacity of ≈81 mAh g^{-1} (≈76% of the initial discharge capacity) is maintained at the 20th cycle. At a relatively high current rate of 20 mA g^{-1}, P3-$K_{0.5}MnO_2$ also retains a reversible capacity of ≈70 mAh g^{-1} (≈70% of the initial discharge capacity) with a coulombic efficiency of ≈95% for 50 cycles when cycled at 1.5–3.9 V (Figure 2f). The relatively low coulombic efficiency is likely attributable to side reactions in K metal anode and electrolytes. The brown/yellow color of the glass fiber separator after 20 cycles most likely results from the side reaction of electrolyte with K metal (Figure S4, Supporting Information). In fact, the high reactivity between K metal and conventional carbonate-based electrolytes, resulting in low coulombic efficiency, is another challenge in KIBs.[12] We further performed rate capability tests of P3-type $K_{0.5}MnO_2$ at various current rates from 10 to 300 mA g^{-1}. Discharge capacities of 97, 87, 82, 72, and 38 mAh g^{-1} are obtained at 10, 30, 50, 100, and 300 mA g^{-1}, respectively (Figure S5, Supporting Information). While the rate capability is respectable, it is lower than in many Li-ion and Na-ion materials. To evaluate whether this is due to poor diffusion of K ions in $K_{0.5}MnO_2$ we evaluated the diffusivity of K ions using galvanostatic intermittent titration technique (GITT) (Figure S6, Supporting Information). The GITT is performed at a current rate of 5 mA g^{-1} with a 2-h relaxation time. The diffusivity is estimated to 10^{-13}–10^{-14} cm^2 s^{-1}, which is lower than Na and Li in layered oxide compounds (10^{-10}–10^{-13} for Na in Na_xMnO_2[13a] and 10^{-10}–10^{-11} for Li in Li_xCoO_2[13b]).

The K-storage mechanism for P3-$K_{0.5}MnO_2$ was investigated using in situ XRD. **Figure 3** presents in situ XRD patterns (2 h scan) collected from the P3-$K_{0.5}MnO_2$ cathode cycled at 2 mA g^{-1}. We observe two-phase reactions in specific narrow K contents ($0.395 < x < 0.425$ and $0.316 < x < 0.364$ in K_xMnO_2) with solid-solution states at other K compositions. The (003) and (006) peaks shift to lower angles upon K extraction (Figure 3b,c), indicating the expansion of the MnO_2 slab distance, as is commonly observed in layered alkali-transition metal-oxide compounds.[10,14] More importantly, the (015) peak disappears and a new (104) peak appears to evolve at $x \approx 0.41$ in K_xMnO_2. Unfortunately, the (104) peak overlaps with a background Al peak at ≈18.5 °; however, the (104) peak develops as a noticeable shoulder-like peak upon K extraction, as observed in scan #7 in Figure 3d–f. This feature indicates a phase transition from a P3 to O3 structure as K ions removed.[14,15] Upon further K-extraction to $x \approx 0.34$ in K_xMnO_2, a new set of XRD peaks to the left of the (003) and (006) peaks appears, as highlighted in Figure 3b,c, indicating the occurrence of another phase transition. We

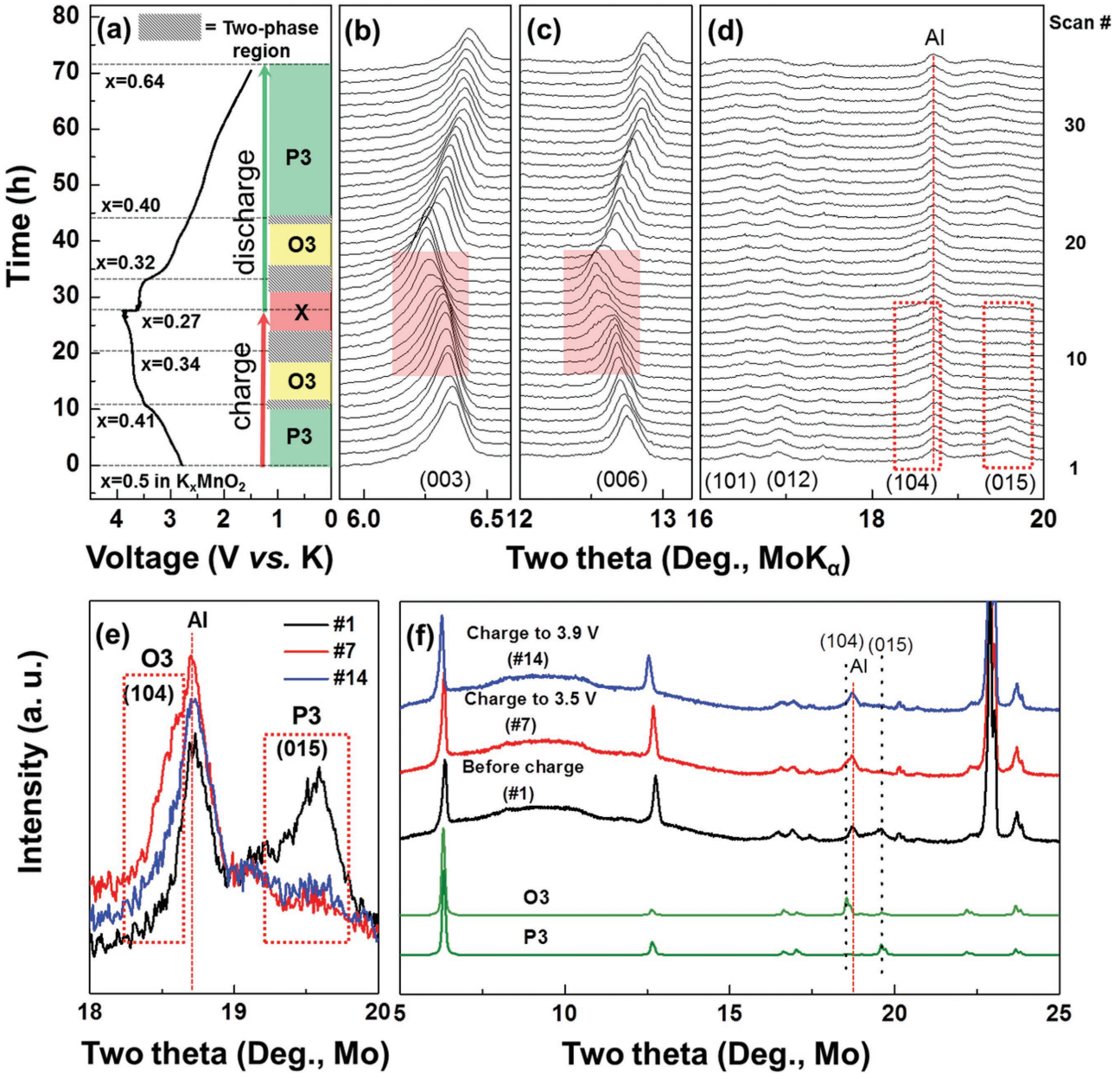

Figure 3. Structural changes of P3-$K_{0.5}MnO_2$ during charge and discharge. a) Typical charge/discharge profiles of P3-type $K_{0.5}MnO_2$ at a current rate of 2 mA g^{-1}. b–d) In situ XRD pattern taken for 2 h scanning rate per pattern. e) XRD peak comparison of as-prepared (scan #1), scan #7, and scan #14 P3-$K_{0.5}MnO_2$ at 18°–20°, in which the (104) and (015) peaks indicate O3 and P3 structures, respectively; and f) comparison with simulated XRD patterns of the O3 and P3 structures. K ions occupy octahedral and prismatic sites in the O3 and P3 structures, respectively. The O3 structure has an ABCABC oxygen stacking sequence, whereas the P3 structure has an ABBCCA oxygen stacking sequence.

expect that these new peaks are still related to the (00*l*) planes and may indicate a two-phase reaction to a phase with larger slab spacing at $0.34 > x > 0.27$. Because of the limited resolution of the in situ XRD and peaks from the background, we defer to explicitly determine the structure of this new phase at high state of charge and denote the phase as "X" However, it should be emphasized that the X phase may maintain O3-like stacking as the shoulder-like (104) peak is still evident; the overall peak intensity near 18.5 ° at $0.34 > x > 0.27$ in K_xMnO_2 (e.g., #14 in Figure 3d–f) is larger than that in P3-$K_{0.5}MnO_2$ (#1), indicating superposition of the (104) peak on the Al background. The phase evolution is reversed during the discharge process with no additional phase transitions when discharging to 1.5 V, suggesting reversible K intercalation and deintercalation behavior in P3-$K_{0.5}MnO_2$. The P3-O3-X transitions can be more clearly seen in the 2D plot of the in situ XRD patterns presented in Figure S7 in the Supporting Information.

To further validate the phase transition with respect to the K content, we computed the formation energies of P3-, O3-, and O1-type K_xMnO_2 structures as a function of the K content ($x = 0.25$, 0.33, 0.5, and 0.66) using DFT. The results are plotted in **Figure 4**a. We considered the P3 (ABBCCA oxygen stacking),

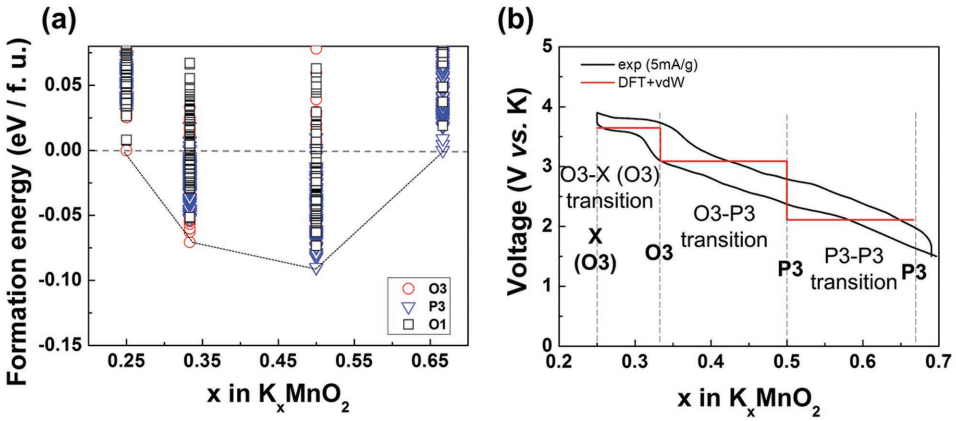

Figure 4. a) Formation energies of P3, O3, and O1 structures for K_xMnO_2 as a function of K content (x) obtained using ab initio DFT calculations. b) Calculated voltage plot (DFT+vdW) compared with experimentally obtained charge/discharge profiles.

O3 (ABCABC oxygen stacking), and O1 (ABAB oxygen stacking) structures as they can transform into each other via sliding of the MnO_2 slab without breaking Mn–O bonds. In Na_xMO_2, a similar P3–O3 phase transition is experimentally observed during electrochemical cycling, and transformation to an O1 structure is sometimes observed at low Na concentrations.[14–16] The computational results indicate that the P3-type framework has the lowest energy at high K content ($x = 0.5$ and 0.66), whereas the O3-type framework becomes stable at low K content ($x = 0.25$ and 0.33), which is consistent with observation of a P3 to O3 transition observed in the in situ XRD. An approximate voltage profile was also calculated from the ground state DFT energies as[17]

$$V = -\frac{E(K_{x1}MnO_2) - E(K_{x2}MnO_2) - (x_2 - x_1)E(K)}{(x_2 - x_1)F} \quad (1)$$

where $E(K_xMnO_2)$ are the DFT energies of the most stable K_xMnO_2 configurations at each composition and $E(K)$ is the energy of bcc K metal (space group: Im–$3m$). F is the Faraday constant. Figure 4b shows calculated voltage profile of K_xMnO_2 (red line) as a function of K contents overlaid with the experimental charged/discharged voltage profile (black line). It should be noted that the DFT calculation approximates the voltage curve by calculating the energy at a limited number of K contents (i. e. $x = 0.25$, 0.33, 0.5, and 0.66 in K_xMnO_2). Between each two compositions only the local average voltage can be obtained.[18] As a result, the flat parts of the calculated voltage profile are artificial as they only represent the averaged voltage between these specific K contents. More detailed voltage curves can in principle be applied by using the cluster expansion technique.[19] However, overall, the calculated voltage profile is in a good agreement with the experimental voltage profile. The large K slab spacing (>4 Å) between the oxide layers necessitates use of the van der Waals (vdW) correction[20] to calculate the voltage profile. Without vdW correction the voltage is under-predicted by about 0.55 V (Figure S8, Supporting Information).

Large alkali ions, such as Na^+ and K^+ have certain advantages over Li^+ ions. In many Li-layered oxide compounds, TM ions migrate into the Li layer upon delithiation, which often results in an irreversible structural change and thus capacity degradation.[21] Layered $LiMnO_2$, for example, is almost completely converted into a spinel structure due to rapid redistribution of Mn into the Li sites.[22] This TM migration through the intermediate tetrahedral site is assisted by Li migration into tetrahedral sites, forming TM_{tet}–Li_{tet} dumbbells.[22a,23] Although TM migration has also been reported in Na systems, usually when more than 0.5 Na is extracted, as observed in $NaFeO_2$, $NaTiO_2$, and $NaCrO_2$,[15,24] this process is energetically more difficult than in the Li systems because the larger size of Na^+ makes it energetically less favorable to form a Na–TM dumbbell.[23] It is highly likely that TM migration is even more difficult in K-layered oxides because of the large K ion radius. In addition, the larger K slab spacing creates highly distorted sites in the alkali layer, making TM migration less favorable, as compared to Na and Li layered materials. This explains at least in part why the structural change upon electrochemical cycling is reversible in K_xMnO_2 for $0.27 < x < 0.70$, as demonstrated by our electrochemical results.

The data in Figure 2 indicates that the voltage range substantially affects the cyclability of the P3-$K_{0.5}MnO_2$ cathode. When charging to 4.2 V, the plateau-like voltage profile observed at ≈4.1 V suggests that the material undergoes a structural change that is different from the P3-O3-X transformation. However, unlike the plateau for the O3-X transformation, this high voltage plateau is less obvious in discharge, and this irreversibility of structural evolution likely impacts the capacity retention. To better understand the nature of phase transformation occurring at ≈4.1 V, we performed in situ XRD for two successive cycles between 1.5 and 4.2 V at a current rate of 7 mA g^{-1} (Figure S9, Supporting Information). Interestingly, the (00l) peaks at 6.5° and 12.5° broaden while their intensity significantly decreases at the top of charge ($x < 0.27$ in K_xMnO_2). This change in the peak profile can originate from stacking faults along the c-axis. The subsequent discharge partially recovers the peak profile, but not perfectly, implying that only some of the stacking changes are reversible. This trend in the (00l) peaks is also observed during the second cycle. As a result, we expect the repeated formation and partial healing of the stacking faults or defects to result in an irreversible structure change. Thus, the voltage range should be carefully tuned to extend the effective lifetime of the P3-$K_{0.5}MnO_2$ cathode.

In summary, we demonstrated P3-structured $K_{0.5}MnO_2$ as a new cathode material for KIBs. This cathode delivers a reversible capacity of ≈100 mAh g^{-1}. Between 1.5 and 3.9 V, K_xMnO_2 cycles through reversible P3-O3-X phase transitions, whereas overcharging to 4.2 V leads to significant capacity loss. This combined experimental and theoretical study on layered $K_{0.5}MnO_2$ provides insight for the design of novel cathode materials and opens up a new path toward the development of high-performance KIBs.

Supporting Information

Supporting Information is available from the Wiley Online Library or from the author.

Acknowledgements

This work was supported by the Laboratory Directed Research and Development Program of Lawrence Berkeley National Laboratory under U.S. Department of Energy (Contract No. DE-AC02-05CH11231). Work at the Molecular Foundry was supported by the Office of Science, Office of Basic Energy Sciences of the US Department of Energy under Contract No. DE-AC02-05CH11231. This work used the Extreme Science and Engineering Discovery Environment (XSEDE), which was supported by National Science Foundation grant no. ACI-1053575, and resources of the National Energy Research Scientific Computing Center (NERSC), a DOE Office of Science User Facility supported by the Office of Science of the US Department of Energy under contract no. DE-AC02-05CH11231. This research was also supported by Basic Science Research Program through the National Research Foundation of Korea (NRF) funded by the Ministry of Education (2017R1A6A3A03001850).

Conflict of Interest

The authors declare no conflict of interest.

Keywords

batteries, energy storage, layered compounds, potassium

Received: May 3, 2017
Revised: June 23, 2017
Published online: August 7, 2017

[1] a) H. Kim, H. Kim, Z. Ding, M. H. Lee, K. Lim, G. Yoon, K. Kang, *Adv. Energy Mater.* **2016**, *6*, 1600943; b) S.-W. Kim, D.-H. Seo, X. Ma, G. Ceder, K. Kang, *Adv. Energy Mater.* **2012**, *2*, 710; c) M. D. Slater, D. Kim, E. Lee, C. S. Johnson, *Adv. Funct. Mater.* **2013**, *23*, 947.

[2] G. Yoon, H. Kim, I. Park, K. Kang, *Adv. Energy Mater.* **2017**, *7*, 1601519.

[3] a) S. Komaba, T. Hasegawa, M. Dahbi, K. Kubota, *Electrochem. Commun.* **2015**, *60*, 172; b) Z. Jian, W. Luo, X. Ji, *J. Am. Chem. Soc.* **2015**, *137*, 11566.

[4] a) Z. Jian, Z. Xing, C. Bommier, Z. Li, X. Ji, *Adv. Energy Mater.* **2016**, *6*, 1501874; b) K. Share, A. P. Cohn, R. Carter, B. Rogers, C. L. Pint, *ACS Nano* **2016**, *10*, 9738; c) H. Kim, G. Yoon, K. Lim, K. Kang, *Chem. Commun.* **2016**, *52*, 12618.

[5] a) W. D. McCulloch, X. Ren, M. Yu, Z. Huang, Y. Wu, *ACS Appl. Mater. Sci.* **2015**, *7*, 26158; b) I. Sultana, T. Ramireddy, M. M. Rahman, Y. Chen, A. M. Glushenkov, *Chem. Commun.* **2016**, *52*, 9279.

[6] a) J. Han, M. Xu, Y. Niu, G.-N. Li, M. Wang, Y. Zhang, M. Jia, C. M. Li, *Chem. Commun.* **2016**, *52*, 11274; b) B. Kishore, G. Venkatesh, N. Munichandraiah, *J. Electrochem. Soc.* **2016**, *163*, A2551.

[7] a) K. Lei, F. Li, C. Mu, J. Wang, Q. Zhao, C. Chen, J. Chen, *Energy Environ. Sci.* **2017**, *10*, 552; b) Q. Deng, J. Pei, C. Fan, J. Ma, B. Cao, C. Li, Y. Jin, L. Wang, J. Li, *Nano Energy* **2017**, *33*, 350.

[8] a) A. Eftekhari, *J. Power Sources* **2004**, *126*, 221; b) C. Vaalma, G. A. Giffin, D. Buchholz, S. Passerini, *J. Electrochem. Soc.* **2016**, *163*, A1295; c) X. Wang, X. Xu, C. Niu, J. Meng, M. Huang, X. Liu, Z. Liu, L. Mai, *Nano Lett.* **2017**, *17*, 544; d) L. Xue, Y. Li, H. Gao, W. Zhou, X. Lü, W. Kaveevivitchai, A. Manthiram, J. B. Goodenough, *J. Am. Chem. Soc.* **2017**, *139*, 2164; e) C. Zhang, Y. Xu, M. Zhou, L. Liang, H. Dong, M. Wu, Y. Yang, Y. Lei, *Adv. Funct. Mater.* **2017**, *27*, 1604307; f) H. Kim, J. C. Kim, S.-H. Bo, T. Shi, D.-H. Kwon, G. Ceder, *Adv. Energy Mater.*, **2017**, 1700098.

[9] C. Delmas, C. Fouassier, *Z. Anorg. Allg. Chem.* **1976**, *420*, 184.

[10] R. Berthelot, D. Carlier, C. Delmas, *Nat. Mater.* **2011**, *10*, 74.

[11] a) Y. Hinuma, Y. S. Meng, G. Ceder, *Phys. Rev. B* **2008**, *77*, 224111; b) V. L. Chevrier, S. P. Ong, R. Armiento, M. K. Y. Chan, G. Ceder, *Phys. Rev. B* **2010**, *82*, 075122.

[12] G. He, L. F. Nazar, *ACS Energy Lett.* **2017**, *2*, 1122.

[13] a) N. Bucher, S. Hartung, J. B. Franklin, A. M. Wise, L. Y. Lim, H.-Y. Chen, J. N. Weker, M. F. Toney, M. Srinivasan, *Chem. Mater.* **2016**, *28*, 2041; b) Y. J. Kim, H. Kim, B. Kim, D. Ahn, J.-G. Lee, T.-J. Kim, D. Son, J. Cho, Y.-W. Kim, B. Park, *Chem. Mater.* **2003**, *15*, 1505.

[14] S. Komaba, N. Yabuuchi, T. Nakayama, A. Ogata, T. Ishikawa, I. Nakai, *Inorg. Chem.* **2012**, *51*, 6211.

[15] S.-H. Bo, X. Li, A. J. Toumar, G. Ceder, *Chem. Mater.* **2016**, *28*, 1419.

[16] D. Yuan, X. Liang, L. Wu, Y. Cao, X. Ai, J. Feng, H. Yang, *Adv. Mater.* **2014**, *26*, 6301.

[17] M. K. Aydinol, A. F. Kohan, G. Ceder, K. Cho, J. Joannopoulos, *Phys. Rev. B* **1997**, *56*, 1354.

[18] M. K. Aydinol, G. Ceder, *J. Power Sources* **1997**, *68*, 664.

[19] a) A. Van der Ven, M. K. Aydinol, G. Ceder, *J. Electrochem. Soc.* **1998**, *145*, 2149; b) M. E. Arroyo y de Dompablo, A. Van der Ven, G. Ceder, *Phys. Rev. B* **2002**, *66*, 064112.

[20] S. Grimme, J. Antony, S. Ehrlich, H. Krieg, *J. Chem. Phys.* **2010**, *132*, 154104.

[21] a) L. A. de Picciotto, M. M. Thackeray, W. I. F. David, P. G. Bruce, J. B. Goodenough, *Mater. Res. Bull.* **1984**, *19*, 1497; b) Y. Shao-Horn, S. A. Hackney, A. R. Armstrong, P. G. Bruce, R. Gitzendanner, C. S. Johnson, M. M. Thackeray, *J. Electrochem. Soc.* **1999**, *146*, 2404; c) Z. Lu, J. R. Dahn, *J. Electrochem. Soc.* **2003**, *150*, A1044.

[22] a) J. Reed, G. Ceder, A. Van Der Ven, *Electrochem. Solid-State Lett.* **2001**, *4*, A78; b) G. Vitins, K. West, *J. Electrochem. Soc.* **1997**, *144*, 2587; c) R. J. Gummow, M. M. Thackeray, *J. Electrochem. Soc.* **1994**, *141*, 1178; d) J. N. Reimers, E. W. Fuller, E. Rossen, J. R. Dahn, *J. Electrochem. Soc.* **1993**, *140*, 3396.

[23] S. Kim, X. Ma, S. P. Ong, G. Ceder, *Phys. Chem. Chem. Phys.* **2012**, *14*, 15571.

[24] a) N. Yabuuchi, H. Yoshida, S. Komaba, *Electrochemistry* **2012**, *80*, 716; b) A. Maazaz, C. Delmas, P. Hagenmuller, *J. Inclusion Phenom.* **1983**, *1*, 45.

